Expansion and crystallization of a sediment of charged colloidal spheres

Jeroen S. van Duijneveldt, Jan K. G. Dhont, and Henk N. W. Lekkerkerker
Van't Hoff Laboratory, Utrecht University, Padualaan 8, 3584 CH Utrecht, The Netherlands

(Received 18 May 1993; accepted 21 July 1993)

An amorphous sediment of charged colloidal particles in a nonaqueous solvent was prepared by centrifugation. The evolution of sediment height and volume fraction profile to equilibrium were studied with light scattering. A simple sedimentation–diffusion equation allows the experimental data to be modeled quantitatively. The top of the sediment crystallizes within a week, whereas the lower part of the sediment does not show any sign of crystallization after several months, indicating a strong concentration dependence of crystallization rate.

I. INTRODUCTION

Detailed information about the thermodynamic properties of colloidal dispersions is contained in the concentration profile at sedimentation equilibrium. Perrin made use of this to determine Boltzmann's constant from the barometric height distribution of noninteracting particles.[1] More generally, information about particle interactions can be obtained from a measured concentration profile[2–4] and it is possible, in principle, to extract the osmotic equation of state.[5] In the present work, the relaxation of a compressed sediment towards equilibrium is studied. Besides information about the equation of state, this also gives insight in the diffusion and crystallization behavior of a concentrated suspension.

As was shown first by Einstein,[6] the diffusion coefficient is equal to a mobility multiplied by the derivative of osmotic pressure with respect to density. Once the osmotic equation of state is known from the equilibrium concentration profile, information about the mobility can, in principle, be obtained by studying the relaxation of the concentration profile towards equilibrium. The feasibility of obtaining the osmotic equation of state directly from a measured concentration profile has been demonstrated with computer simulations by Barrat *et al.*[5] The application of this method to colloidal dispersions will, however, depend on an accurate measurement of the concentration profile. An alternative procedure, also incorporating the time evolution of the concentration profile, is to start from model expressions for the equation of state and the mobility. A sedimentation–diffusion equation can then be constructed from which the concentration profile as a function of time is calculated. A comparison with experimental profiles then serves to test the model expressions. This has been done by Davis and Russel for the settling of hard spheres.[7,8]

In dispersions of spherical particles that are sufficiently monodisperse, crystallization may occur on increasing concentration (see, for instance, Ref. 9). When a sediment of such particles is formed, starting from a homogeneous dispersion, a crystalline phase can grow provided that the sedimentation rate is not too high compared to the crystallization rate. For hard spheres, this has been treated quantitatively using a sedimentation–diffusion equation[10] and observed experimentally.[11,12] For charged particles, the formation of an ordered sediment has also been observed.[13]

In this work, we extend the sedimentation–diffusion model of Davis and Russel to describe a dispersion of charged particles. We apply this model to an amorphous sediment of charged colloidal particles in a nonaqueous solvent. The sediment is produced by centrifugation and then relaxation under normal gravity is studied. In one week the sediment expands and crystallization occurs in the top layer of the sediment. Light scattering is used to monitor sediment height and structure as a function of time.

To calculate the equilibrium density profile, the osmotic equation of state of the dispersion needs to be known. For the particles used here, the interaction potential contains two important contributions: a hard-core repulsion at contact and a long-range repulsion due to electrostatic interactions. On the one hand, the thermodynamic properties of hard spheres have been studied extensively. Of particular relevance here is the work of Woodcock on the equation of state of the (metastable) disordered phase at high density.[14] On the other hand, the properties of point particles interacting via a screened Coulomb repulsion (a Yukawa potential) have been studied theoretically[15] and by computer simulation.[16,17] For our particles both the long-range repulsion and the hard-core interaction need to be taken into account. We therefore present a simple hard-sphere perturbation theory pertinent to our particles. It is incorporated in a sedimentation-diffusion equation in Sec. II to calculate the dynamics of expansion as well as the equilibrium profile.

The experimental procedure is described in Sec. III and the structure factor of the sediment as function of height and time is presented in Sec. IV. In Sec. V experimental data are compared with the sedimentation–diffusion model. Finally, some remarks about the sediment structure are made in Sec. VI.

II. THEORY

A. Diffusion equation

In this section a diffusion equation for interacting particles in an external force field is obtained using irreversible thermodynamics.[2,18,19] A detailed discussion of the application of this equation to the sedimentation of hard spheres

 0021-9606/93/99(9)/6941/9/$6.00

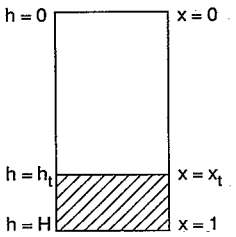

FIG. 1. Schematic of the sample.

has been given by Russel and co-workers.[20] This equation applies to the present case of an expanding sediment as well.

We consider a sediment of height h_t contained in a liquid volume of height H (see Fig. 1). The change of particle number density ρ with time t' is given by

$$\frac{\partial \rho}{\partial t'}=-\frac{\partial}{\partial h}J=-\frac{\partial}{\partial h}\rho b\mathscr{K}, \tag{1}$$

where the flux J is the density multiplied by the mobility b and the driving force $\mathscr{K}$. This driving force is the sum of the gravitational force and the Brownian force, expressed here as a function of the osmotic pressure of the particles, Π:

$$\mathscr{K}=F_g-\frac{1}{\rho}\frac{\partial \Pi}{\partial \rho}\frac{\partial \rho}{\partial h}. \tag{2}$$

In the following, we assume that the particles are monodisperse spheres of radius a and density ρ_p suspended in a liquid of density ρ_0. Then,

$$F_g=\tfrac{4}{3}\pi a^3(\rho_p-\rho_0)g, \tag{3}$$

where $g=9.81\ \mathrm{ms}^{-2}$ is the gravitational acceleration. The mobility is written as function of the volume fraction $\phi=\frac{4}{3}\pi a^3\rho$ and solvent viscosity η,

$$b(\phi)=\frac{K(\phi)}{6\pi\eta a}. \tag{4}$$

The function $K(\phi)$ depends on particle interactions. At infinite dilution $K=1$. Using Eqs. (2)–(4) and defining the compressibility factor $Z=\Pi/\rho k_BT$ (with temperature T and Boltzmann constant k_B) Eq. (1) becomes

$$\frac{\partial \rho}{\partial t'}=\frac{\partial}{\partial h}b\left(k_BT\frac{d}{d\phi}[\phi Z(\phi)]\frac{\partial \rho}{\partial h}-\rho F_g\right). \tag{5}$$

Introducing the Péclet number $\mathrm{Pe}=F_gH/k_BT$ and switching to reduced variables

$$x=h/H, \quad t=t'F_gb(0)/H,$$

a dimensionless equation is obtained from Eq. (5),

$$\frac{\partial \phi}{\partial t}=\frac{\partial}{\partial x}\left(\frac{D(\phi)}{\mathrm{Pe}}\frac{\partial \phi}{\partial x}-\phi K(\phi)\right), \quad 0<x<1. \tag{6}$$

The dimensionless diffusivity $D(\phi)$ is given by the generalized Stokes–Einstein equation

$$D(\phi)=K(\phi)\frac{d}{d\phi}[\phi Z(\phi)]. \tag{7}$$

At the boundaries $x=0$ and $x=1$ the flux should be zero;

$$f(\phi)=\phi K(\phi)-\frac{D(\phi)}{\mathrm{Pe}}\frac{\partial \phi}{\partial x}=0, \quad x=0 \text{ or } 1,\ t>0. \tag{8}$$

To complete the problem, the initial density profile $\phi(x;t=0)$ has to be specified.

B. Charged particles

To solve Eq. (6), expressions are needed for $Z(\phi)$ and $K(\phi)$ of charged, spherical particles surrounded by an electrical double layer. The pair interaction of such particles is given by the Derjaguin–Landau–Verwey–Overbeek (DLVO) theory.[21] When van der Waals forces are neglected, which is reasonable in this case since the particles are in a refractive index-matching solvent, a purely repulsive potential remains. This potential consists of a hard repulsion due to the core particles and a more slowly decaying double layer interaction. When the cores are treated as point particles a Yukawa potential results. This approximation is expected to be valid at low particle densities. Tejero *et al.*[15] have recently described a procedure for calculating the compressibility factor for Yukawa particles. They use the Rogers–Young integral equation for the fluid phase and a hard-sphere perturbation theory for the solid phase.

In the present case, however, the particles form a dense sediment and the point-particle approximation is likely to break down.[22] We therefore develop a simple hard-sphere perturbation theory separating the pair interaction into a hard-sphere repulsion V_{HS} and a double layer repulsion V_{DL};

$$\begin{aligned} &V=V_{\mathrm{HS}}+V_{\mathrm{DL}},\\ &V_{\mathrm{HS}}=\infty, \quad r\leqslant\sigma=2a,\\ &V_{\mathrm{HS}}=0, \quad r>\sigma. \end{aligned} \tag{9}$$

More accurate results would probably be obtained by using the sophisticated prescription for splitting up the pair potential in Ref. 23. In our study the double layer thickness κ^{-1} is thin compared to the particles, so $\kappa a\gg 1$. The interaction of two spherical double layers is then approximated by[21]

$$\begin{aligned} &V_{\mathrm{DL}}=C\ln(1+e^{-\kappa(r-\sigma)}), \quad r>\sigma,\\ &C=\pi\epsilon\epsilon_0\psi_0^2\sigma, \end{aligned} \tag{10}$$

where ψ_0 is the surface potential and $\epsilon\epsilon_0$ the dielectric permittivity of the solvent. Both κ and ψ_0 are taken to be constants but will depend on ϕ in general, for instance, κ^{-1} will decrease with ϕ due to the increasing counter ion concentration.

The configurational part of the partition function of N particles in the canonical ensemble is given by

$$Q_{NVT}=\int e^{-\beta[V_{\mathrm{HS}}(r^N)+V_{\mathrm{DL}}(r^N)]}dr^N, \tag{11}$$

where $\mathbf{r}^N$ represents all 3 N particle coordinates. The calculation of the integral can be simplified considerably by approximating $V_{DL}(\mathbf{r}^N)$ by its value in a static lattice, $\langle V_{DL}(\mathbf{r}^N)\rangle_s$.[15] Using $P=k_BT\partial \ln(Q_{NVT})/\partial V$, we obtain

$$Z=Z_{HS}+\frac{\rho}{Nk_BT}\frac{\partial}{\partial\rho}\langle V_{DL}(\mathbf{r}^N)\rangle_s. \tag{12}$$

Initially, the rapidly formed sediment is amorphous. For hard spheres, the compressibility factor is then approximated by[14]

$$Z_{HS}=\frac{3\phi_m}{\phi_m-\phi}, \tag{13}$$

where the Bernal glass density is used, $\phi_m=0.64$. To calculate the double layer interaction, we assume each particle to be surrounded by n neighbors at the same distance r_n so

$$\langle V_{DL}(\mathbf{r}^N)\rangle_s=\frac{n}{2}NV_{DL}(r_n). \tag{14}$$

For $\kappa a\gg 1$ it is sufficient to consider nearest neighbors only. At close packing ($\phi=\phi_m$), we assume that the particles touch, $\sigma=r_n$, which leads to the scaling

$$\frac{r_n}{\sigma}=\left(\frac{\phi}{\phi_m}\right)^{-1/3}. \tag{15}$$

Substitution of Eqs. (13)–(15) in Eq. (12) yields

$$Z(\phi)=\frac{3\phi_m}{\phi_m-\phi}+\frac{n}{6}\beta C\frac{\kappa r_n e^{-\kappa(r_n-\sigma)}}{1+e^{-\kappa(r_n-\sigma)}}. \tag{16}$$

with $\beta=1/k_BT$. For the amorphous system $n=12$ is taken.[24] The same value would apply to an fcc crystal. In order to apply the same equations to an fcc crystal, the only change would be to put $\phi_m=0.74$.[25]

Although this derivation supposes that the particles are in a dense packing, it is assumed that the resulting density profiles are determined mainly by the compressibility factor at high densities so Eq. (16) may be used at all ϕ. Furthermore, the change of the compressibility factor as the sediment crystallizes is neglected. As the fcc crystal has $\phi_m=0.74$, this change may be important at high ϕ. This will be discussed later.

It still remains necessary to specify $K(\phi)$. Even for hard spheres this is not a trivial problem. An empirical expression providing reasonable results over the entire volume fraction range for hard spheres is

$$K(\phi)=(1-\phi)^\nu \tag{17}$$

with $\nu=4.9$.[26] For charged particles K is expected to show a different behavior,[27,28] going down more steeply at low concentrations but approaching the hard-sphere result again at higher concentrations. In the present study, we still use Eq. (17), with ν as an adjustable parameter. It has been tacitly assumed that friction due to the electrical double layer may be neglected.

TABLE I. Model parameters.

Pe	1.2×10^4
$\kappa\sigma$	14
ϕ_0	0.155
βC	2.3×10^2
ν	6

C. Model predictions

Starting with an initial density profile its time evolution can be calculated from Eq. (6). An equation for the equilibrium profile is obtained by putting $d\phi/dt=0$ in Eq. (6):

$$\frac{D(\phi)}{\mathrm{Pe}}\frac{\partial\phi}{\partial x}=\phi K(\phi). \tag{18}$$

The gravitational force on the particles is balanced by an osmotic pressure increase with height in the sample, giving the boundary condition

$$\phi(1)Z[\phi(1)]-\phi(0)Z[\phi(0)]=\phi_0\mathrm{Pe}, \tag{19}$$

where ϕ_0 is the overall particle volume fraction (the total volume of all particles divided by the available volume). For high Pe and low ϕ_0 it is safe to neglect $\phi(0)$ and Eq. (19) can be solved for $\phi(1)$. The density profile is then given by

$$\mathrm{Pe}(1-x)=\left[\frac{3\phi_m}{\phi_m-\phi}+3\ln\frac{\phi}{\phi_m-\phi}-2\beta C\left(3\kappa r_n-3\ln(1+e^{\kappa(r_n-\sigma)})-\frac{\kappa r_n}{1+e^{\kappa(r_n-\sigma)}}\right)\right]_{\phi}^{\phi(1)}. \tag{20}$$

When $\phi(0)$ cannot be neglected, an iterative procedure can be adopted to obtain $\phi(1)$.

The parameters used to model the experiments are given in Table I. The values of Pe, $\kappa\sigma$, and ϕ_0 were kept fixed, whereas C and ν were adjusted to fit the experimental data as described later. In Fig. 2 the effect is shown of varying βC, the dimensionless surface potential. For $\mathrm{Pe}=1.2\times10^4$ the volume fraction changes rapidly near the top of the sediment for hard spheres ($C=0$). As C is increased, the profile becomes more extended and the volume fraction changes less abruptly. Nevertheless, the volume fraction always changes rapidly near the top of the sediment.

To model the experimental situation, the expansion of a compressed sediment, the equilibrium profile was calculated using the parameters given in Table I but with $\mathrm{Pe}=6\times10^6$ (corresponding to centrifugation at 500 g). The resulting volume fraction profile was almost a step function. It was used as initial profile. The time evolution at $\mathrm{Pe}=1.2\times10^4$ was then obtained by numerically integrating Eq. (6) with a resolution $\Delta x=5\times10^{-6}$ and relative accuracy in the time direction 10^{-5}. As is shown in Fig. 3 the expansion begins at the top of the sediment and then progressively extends lower into the sediment. The profiles at $t=10$ and at equilibrium are almost indistinguishable.

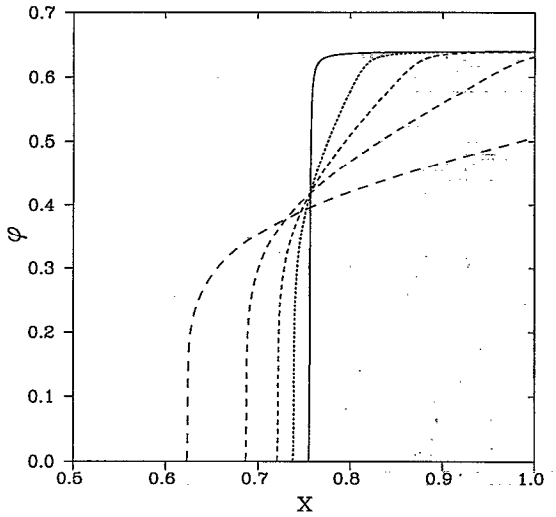

FIG. 2. Calculated equilibrium density profiles for $Pe=1.2\times10^4$, $\kappa\sigma=14$, and $\phi_0=0.155$. The solid line has $\beta C=0$ and the four dashed lines have $\beta C=50$, $\beta C=100$, $\beta C=200$, and $\beta C=500$.

TABLE II. Sample properties.

Solvent	Composition	0.74/0.26 (*w/w*) toluene/ethanol
	Density	$\rho_0=0.846$ g/ml
	Refractive index	$n_D=1.4583$
		$n_{647}=1.4550$
	Dielectric constant	$\epsilon=10$[a]
	Viscosity	$\eta=0.7$ cP[b]
	Temperature	$T=293$ K
Particles	Laboratory code	SCA15(0)TPM
	Radius	$a=353$ nm[c]
	Polydispersity	6%
	Density	$\rho_p=2.0$ g/ml[a]
	Freezing volume fraction	$\phi_F=0.159$
	Melting volume fraction	$\phi_M=0.167$
Sample	Volume fraction	$\phi_0=0.155$
	Volume	1.90 ml

[a]Estimated.
[b]From Ref. 31.
[c]Determined by static light scattering in ethanol.

III. EXPERIMENT

Particles with laboratory code SCA15(0)TPM were synthesized according to Ref. 29. Particle properties are listed in Table II. An estimate was used for the specific weight of the particles since the amount of particles was not sufficient for an accurate measurement. Analytical grade solvents were used as received. The particles were dispersed in a mixture of ethanol and toluene in which the particles were nearly refractive-index matched, such that the first minimum of the particle form factor $P(K)$ was at wave vector $K=1.2\times10^7$ m^{-1}. In this way the form factor minimum did not interfere with the measurement of any structure factor peaks in the sediment. Volume fractions were calculated using the solid content of the sample and the densities given in Table II.

The phase behavior was studied by vortex mixing a sample to destroy all crystallites present and noting its aspect after 1 h. At later time bulk sedimentation occurred. At $\phi>0.18$ no crystallization was visible after 1 h. For $0.167<\phi<0.18$ crystallites formed homogeneously throughout the sample; near the meniscus, larger crystallites were visible in some cases. Below the melting concentration, $\phi_M=0.167$, the crystallites occupied only a part of the total volume. Measurement of the crystalline volume fraction was complicated by a more dense crystalline layer, formed at the bottom due to sedimentation. At the freezing point $\phi_F=0.159$ only a dense crystalline layer at the bottom of the sample was seen, which is ascribed to sedimentation followed by crystallization.

The static light scattering setup allowed simultaneous measurement at scattering angles θ ranging from 17° to 156° with a resolution of 1°. Details can be found in Ref. 30. Samples were prepared in cylindrical round-bottom cuvettes of 1.0 cm diameter. Light with a wavelength $\lambda=647.1$ nm from a Spectra Physics Series 2000 Krypton ion laser was used. The incoming laser beam was attenuated to 20 mW and focused onto a spot of about 0.1 mm diameter on the sample to obtain a sufficient height resolution. To improve statistics the sample was rotated at 0.02 Hz and measurements were averaged over an integer (2–5) number of revolutions. A micrometer screw permitted height adjustment of the sample with an accuracy of 0.01 mm. The thermostatting bath was filled with cyclo-octane and kept at 20 °C. This liquid was chosen since the refractive index ($n^{20}_{647}=1.4558$) was very close to that of the sample, thus reducing smearing of the scattered intensity. The background intensity was measured in the clear liquid above the sediment and substracted. After the experiment the sample was shaken gently to produce a dilute dispersion above the sediment. The scattered intensity of this dispersion was used as form factor of the particles. Assum-

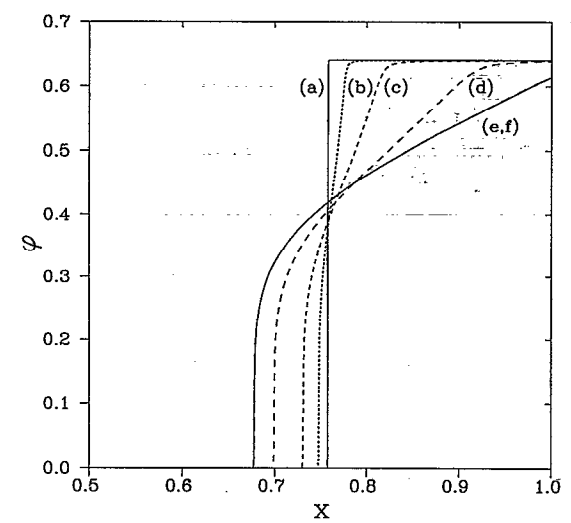

FIG. 3. Expansion of a sediment compressed at $Pe=6\times10^6$ for the parameters given in Table I. Solid lines are calculated from Eq. (20) and dashed lines from numerical integration of Eq. (6). (a) $t=0$; (b) $t=0.01$; (c) $t=0.1$; (d) $t=1$; (e) $t=10$; (f) equilibrium.

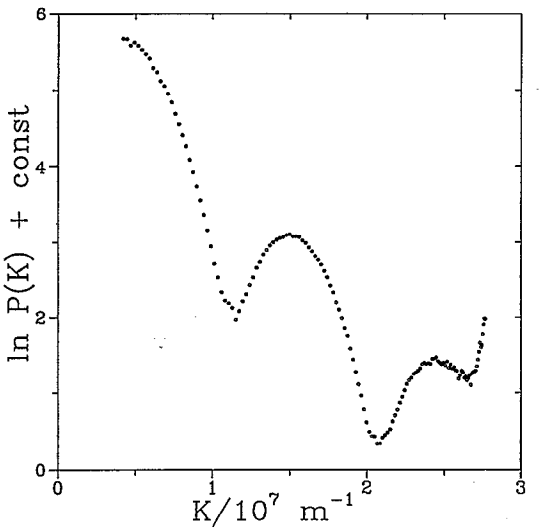

FIG. 4. Form factor of the colloidal particles in ethanol–toluene mixture.

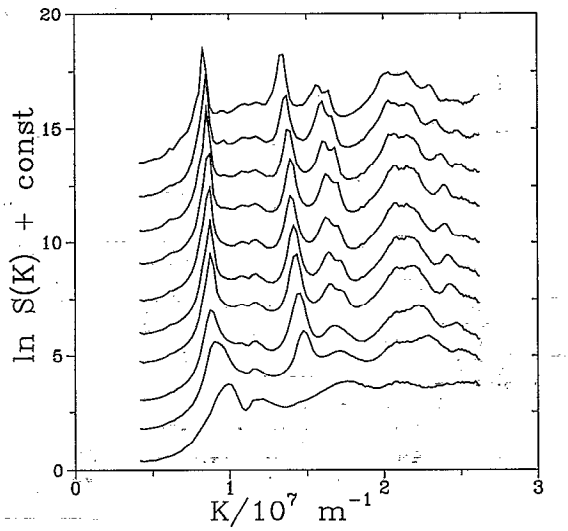

FIG. 5. Scattering curves at $h-h_t=0.8$ mm for time after centrifugation 10 min (lower); 1 h, 1.5 h, 4.5 h, 5.5 h, 7 h, 10.3 h, 25 h, 31 h, and 197 h (upper). Successive curves are shifted by 1.5.

ing that multiple scattering was avoided by refractive index matching, the structure factor in the sediment was calculated from

$$I(K) \propto S(K)P(K). \tag{21}$$

The form factor of the particles in the ethanol-toluene mixture is shown in Fig. 4. At large wave vector the curve is distorted due to stray light, for instance light scattered from the thermostatting bath wall. The last 20 channels have therefore been omitted in further analysis. Inside the sediment the concentration is not known so the measured $S(K)$ contains an unknown proportionality factor. Therefore no effort was made to measure absolute intensities.

IV. EXPANDING SEDIMENT

A sample was prepared just below the freezing concentration, at $\phi_0=0.155$. After vortex mixing a sediment was formed by centrifugation at 500 g for 30 min. The sample was transferred to the light scattering setup and scattering curves were measured at several heights in the sediment during one week. The position of the top of the sediment was noted as well; scattering curves were taken at fixed distances from the top of the sediment.

First some qualitative remarks about the expanding sediment are made. Before the sample was put in the scattering apparatus, it had a homogeneous appearance but a thin layer ($\sim$0.1 mm) of crystallites was visible at the top of the sediment. The sediment was seen to expand, rapidly during the first hours and then gradually more slowly. Starting the experiments 10 min after centrifugation, the sediment expanded in total by 1.7 mm after which the height remained constant. At the same time crystallites were seen, both visually and by light scattering, to grow in the upper region of the sediment. After one week the top 2.3 mm of the sediment contained crystallites. Even after many months the thickness of the crystalline layer did not increase visibly. Careful inspection showed, however, that under certain angles Bragg reflections did become visible in the lower part of the sediment. This was probably due to ordering against the glass wall.

The development of structure 0.8 mm below the top of the sediment is shown in Fig. 5. Because $S(K)$ is measured in arbitrary units ln $S(K)$ is plotted to allow direct comparison of peak shapes. At $K\approx 1.2\times 10^7$ m^{-1} a small peak is visible that, contrary to the other peaks in $S(K)$, does not shift in time. At the same wave vector $P(K)$ is a minimum. Probably some multiple scattering occurs that causes this peak in $S(K)$, as calculated with Eq. (21). In the first experiment (10 min after centrifugation), a glassy structure is observed, dominated by a broad first peak at $Ka\approx 4$. Within 1 h crystallization is seen to occur. The first peak in $S(K)$ becomes more narrow and new Bragg peaks appear at higher wave vector. After 4.5 h the structure seems to remain essentially unchanged. Closer inspection reveals that the Bragg peaks continue to shift towards smaller wave vector. This can be explained by the continuing expansion of the sediment. The sediment structure will be analyzed in more detail in Sec. VI.

In Fig. 6 a scan through the sediment is shown, 197 h after centrifugation. Crystalline peaks are seen in the top 2.3 mm of the sediment. Lower in the sediment a glassy structure is present. The structure factor peak continues to shift to higher wave vectors lower in the sediment, indicating an increase in particle density.

Apparently crystallization is very slow at high volume fraction. As a further test a second sample similar to the first one was prepared. After centrifugation the supernatant was removed and the sample sealed. Using the model described in Sec. II, the overall volume fraction was estimated to be $\phi_0=0.60$ with $H=7$ mm (ϕ_0 is slightly lower than the maximum density, $\phi_m=0.64$, since a rapid initial expansion takes place during the first minutes after centrifugation). Due to gravity a density gradient developed in this sample, but expansion could not take place. The pres-

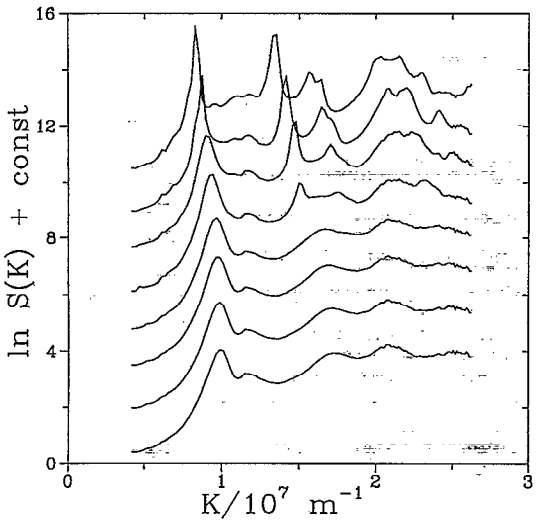

FIG. 6. Scan of the sediment structure 197 h after centrifugation at $h-h_t$ 4.3 mm (lower) to 0.8 mm (upper) with increments of 0.5 mm. Successive curves are shifted by 1.5.

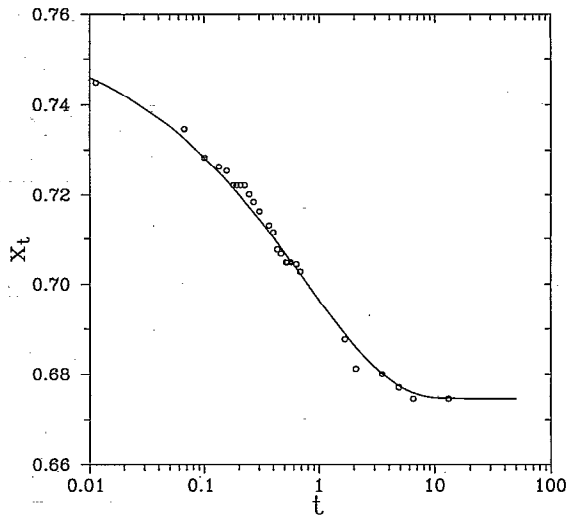

FIG. 7. Position of top of sediment, x_t, as a function of time after centrifugation. Circles: experiments. Solid line: calculated results for parameters shown in Table I.

ence of a gradient was demonstrated by a height dependence of K_1 in the top 2 mm of the sediment. Even after six months the bulk of this sample did not show signs of crystallization. Again very weak Bragg reflections could be seen under certain angles, probably due to ordering against the cell wall. This sample was not fluid and was probably already in a glassy state. The equilibrium concentration profile for this sample, calculated with Eq. (20), had $\phi(0)=0.51$ and $\phi(1)\sim 0.64$.

V. COMPARISON WITH DIFFUSION MODEL

In order to compare the experiments to the model of Sec. II, the model parameters have to be determined. As the sample had a round bottom the model (Fig. 1) was not applicable strictly. We neglect this difference and take the sample to be cylindrical with an equivalent height $H=24.2$ mm obtained by dividing the total sample volume by the cross section of the sample tube. The position in the sample corresponding to $x=1$ was not known accurately due to this procedure and was taken as an adjustable parameter. An alternative choice would be to let $x=1$ correspond to the absolute bottom of the sample. This would be the most proper choice to describe the sedimentation equilibrium. However, in this way the total amount of particles would be incorrect, since the corners of the rectangular cell used in the model would not be present in the round-bottomed tube used in the experiment. From the data in Table II $\mathrm{Pe}=1.2\times 10^4$ and the unit of time $H/F_g b(0)=15.0$ h.

To reproduce the total sediment expansion, starting 10 min after centrifugation, $\beta C=2.3\times 10^2$ had to be chosen [using Eq. (11) this corresponds to $\psi_0=69$ mV]. The offset for the height of the sample was then chosen such that the top of the sediment at long time would coincide with the calculated value. Numerically, the top of the sediment, x_t, was chosen such that $\phi(x_t)=10^{-6}$. As shown in Fig. 7 the calculated curve for $\nu=6$ fits the experimental data rather well. The diffusivity $D(\phi)$ for the parameters given in Table I is compared with the corresponding hard cores ($\beta C=0$) in Fig. 8. Whereas $D(\phi)$ becomes large for hard spheres only near $\phi=\phi_m$, it is large at intermediate ϕ as well for charged spheres.

The measured structure factor provides information about the volume fraction. For a closed-packed structure (fcc, hcp, or a random mixture of these) the relation between the volume fraction and the wave vector of the first Bragg peak, K_1, is

$$\phi=(2/9\sqrt{3\pi^2})(K_1 a)^3. \tag{22}$$

A different equation is needed for an amorphous structure. At present we do not have such an equation available and Eq. (22) will be used at all densities.

In Fig. 9 the calculated equilibrium profile is compared with experimental data taken 197 h after centrifugation.

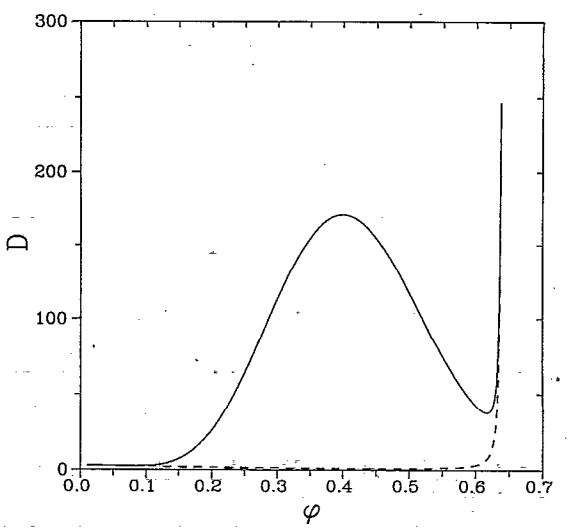

FIG. 8. Dimensionless diffusivity $D(\phi)$ for parameters given in Table I (solid line) and for the hard cores only (dashed line).

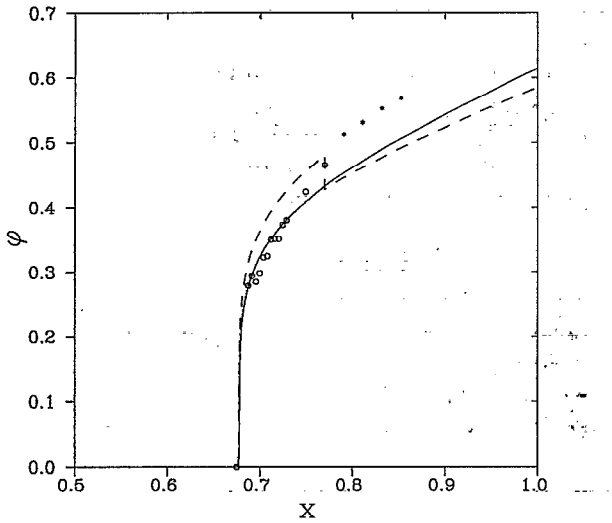

FIG. 9. Equilibrium profile. Solid line, calculated using parameters in Table I; dashed line, crystalline top layer and amorphous bottom layer with parameters as in Table I but with $\beta C=275$. Data taken 197 h after centrifugation and analyzed with Eq. (22). Circles, crystalline structure; asterisks, amorphous structure.

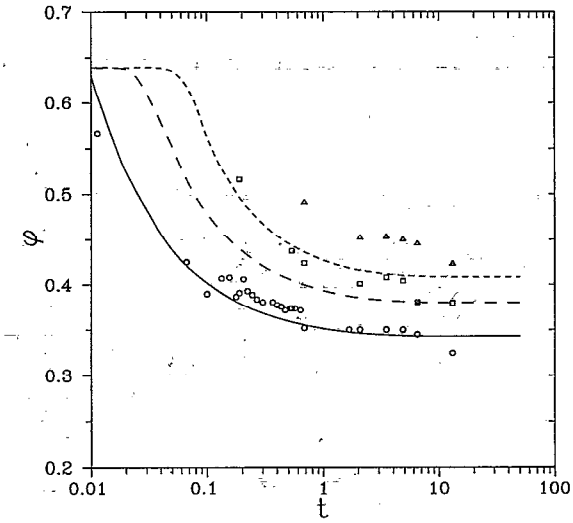

FIG. 10. Experimental and calculated volume fraction vs time contours for $h-h_t=0.8$ mm (circles and solid line), 1.3 mm (squares and medium-dashed line), and 1.8 mm (triangles and dashed line).

The four scattering curves taken deepest inside the sediment did not show any Bragg peaks (see Fig. 6). The use of Eq. (22) is therefore doubtful for these four curves and the corresponding volume fractions are indicated with asterisks in Fig. 9. These four experimental points are found to lie much above the predicted volume fraction profile.

The particles studied here are charged and, therefore, they will tend to be apart as far as possible. In a close-packed crystalline arrangement each particle has 12 identical neighbors in the first coordination shell. In a random (glassy) arrangement the packing is less efficient and at equal volume fraction the particles will be less far apart than in the crystal. The location of the first structure factor peak will be determined by this interparticle spacing and therefore it can be understood qualitatively that the volume fraction calculated with Eq. (22) is too high for a glassy structure.

The scattering curves taken in the top layer of the sediment show Bragg peaks and therefore the use of Eq. (22) seems more appropriate. The volume fractions thus obtained, indicated with circles in Fig. 9, agree rather well with the predicted volume fractions.

So far, all volume fraction profiles have been calculated using Eqs. (15) and (16). When crystallization occurs, a different expression for the osmotic pressure is needed. As already mentioned in Sec. II, it is sufficient here to use the old equations with $\phi_m=0.74$ (for a close-packed structure). The osmotic pressure at equal volume fraction will then be lower than in the amorphous structure. In an attempt to improve on the description of the sediment, this crystalline equation of state was used for the top 2.3 mm of the sediment. The result is shown in Fig. 9 (dashed line). A slightly higher value for the dimensionless particle charge had to be used ($\beta C=275$) to obtain the same total sediment volume as before. At the boundary between the crystalline and the amorphous structure the volume fraction profile is discontinuous, since the osmotic pressure has to be the same on both sides of the boundary.

This approach is seen to produce a slightly better description of the top of the sediment (note that the offset for the x value of the data is uncertain so only the shape of the $\phi-x$ curves should be compared). However, in Fig. 6 it can be seen that the transition between crystalline and amorphous structures is not sudden but rather gradual in fact. Furthermore, the crystalline layer is almost absent at the beginning of the experiment and grows while the expansion takes place. Therefore, a realistic description of the sediment appears to be very complicated. At the beginning of the experiment, the sediment is mainly amorphous and the equilibrium volume fraction profile is reproduced rather well by the amorphous equation of state. Therefore, we will use this equation of state below for the calculation of the time evolution of the volume fraction profile.

The calculated volume fraction profile drops steeply from 0.25 (inside the crystalline region) to zero. This explains the observation that crystallites are seen at the top of the sediment. For similar but smaller ($a\sim 200$ nm) particles a thin turbid layer has been observed on top of the crystalline sediment. For these particles the model predicts a much less steep decay of the volume fraction near the top of the sediment and a layer of about 0.5 mm exists where $\phi<0.13$, the volume fraction of the coexistent crystal for these particles.[31]

The change of volume fraction with time at three values of $h-h_t$ is shown in Fig. 10. Calculated curves and experimental data agree quantitatively only near the top of the sediment and at long times. Again this is probably due to the limited applicability of Eq. (22).

VI. SEDIMENT STRUCTURE

To obtain information about the structure of the sediment, a comparison is made with calculated structure fac-

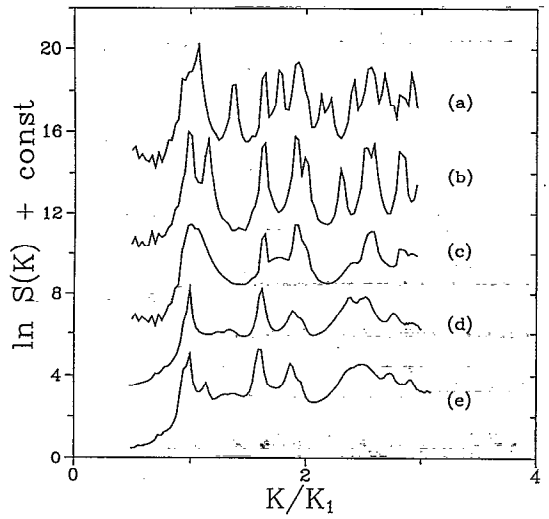

FIG. 11. Calculated $S(K)$ for cubic crystallites with an edge of 20 unit cells: (a) hcp, (b) fcc, and (c) fully disordered mixture fcc/hcp. Experimental curves taken at $h-h_t=1.3$ mm. (d) Expanding sediment after 197 h and (e) sediment formed at 1 g. For comparison, wave vectors are normalized on K_1.

tors. For hard spheres the equilibrium crystal phase is often quoted to be fcc but the free energy difference between fcc and hcp is negligible.[32] For Yukawa particles a bcc structure may form instead of fcc (or perhaps hcp) when the interaction range is long and temperature low.[15–17,33] For the type of particles used here the interaction is screened to such an extent that a close packed structure is observed always.

For colloidal hard spheres it has been found that, at high volume fraction, crystallization may produce a structure intermediate between fcc and hcp stacking, for which the arrangement of close-packed layers is (partially) disordered.[34] Crystals grown slowly show a tendency towards fcc stacking.

To test the possibility of stacking disorder in the sediment structure factors have been calculated for a cubic crystalline with an edge of 20 unit cells, which for the particles used here corresponds to 25 μm at $\phi=0.4$. In Fig. 11 results are shown for fcc, hcp, or a fully disordered stacking; for comparison with experiments $\ln S(K)$ is drawn. These structure factors are averaged over all crystal orientations.[35] The fully disordered stacking produces Bragg peaks only for K values where both fcc and hcp would give a peak. In Fig. 11 experimental data are shown at $h-h_t=1.3$ mm for the expanding sediment after 197 h as well as for a sediment formed under normal gravitational settling from a homogeneous dispersion. The structure of the expanding sediment resembles most the fully disordered structure. The scattering curve of the sediment formed at 1 g is slightly different. In particular, a peak at $K/K_1=1.1$ is present, indicating fcc stacking. Unfortunately, the quality of the experimental data does not allow a detailed comparison with calculated structure factors.

The gravitational field will compress the crystals, thus the lattice parameter will become anisotropic. In addition to this the density gradient near the top of the sediment may influence the crystallization process. The importance of such effects can be assessed by measuring light scattering, not only in the horizontal plane, but also in a vertical plane. Our experimental setup does not allow for such measurements. As judged from visual observations the crystallites did not have any preferred orientation.

VII. DISCUSSION AND CONCLUSIONS

As can be seen in Fig. 2, the particle charge (or surface potential) has a large effect on the equilibrium sediment density profile. The experimental data were fit reasonably well with $\beta C=230$. Using Eq. (11) this corresponds to $\psi_0=69$ mV. For similar dispersions ψ_0 has been reported to be ~ 60 mV.[36,37] Note, however, that assumptions leading to Eq. (16) are compensated for by adjusting C. It would therefore be desirable to test Eq. (16) against results of more realistic calculations or computer simulations. Then a quantitative comparison with experimental data becomes possible.

Experimentally, it is known that, for a given particle size (or Péclet number), the fluidity of a sediment is a rough indicator of the presence of charges on the particles. This can be understood from the marked dependence of the density profile on particle charge, predicted here.

The overall expansion velocity of the sediment is described rather well with $\nu=6$. Therefore the overall mobility is only slightly lower than for hard spheres, where $\nu=4.9$ was found to provide reasonable results at all volume fractions.[26] The lower mobility is expected, since the long-range repulsion of charged particles keeps them further apart on the average than hard spheres, causing a stronger friction due to back flow of solvent. Note that the functional form of Eq. (17) is not really suited for charged particles; at low volume fraction the decrease of K with ϕ is much steeper than predicted with $\nu=6$.[27,28] Whereas the overall mobility of these charged particles appears to differ little from that of hard spheres, the diffusivity $D(\phi)$ is much larger (Fig. 8) due to the higher osmotic pressure.

Near the top of the sediment crystallization occurs. Lower in the sediment ($h-h_t>2.3$ mm) no evidence of crystallization is seen after one week (Fig. 6). Using Fig. 9 the part that does not crystallize would correspond approximately to $\phi>0.45$. When the sample is kept for a few months the crystalline layer remains clearly distinct from the lower part of the sediment and the thickness does not increase noticeably. This compares well with the experiment with the concentrated, sealed sample; it did not show crystallization after six months at calculated $\phi>0.51$. Apparently, the growth of crystals in the bulk of the sample becomes extremely slow at $\phi\sim 0.45$. Nevertheless weak Bragg peaks are seen to develop in the lower part of the sediment at long times, probably due to ordering against the glass wall. This suggests that although crystallization may be very slow, it has not stopped altogether. It has been noted previously by several authors that crystallization kinetics in concentrated colloidal dispersions are very concentration dependent and that the optimum concentration is near the melting concentration.[36,38,39]

The structure factors indicate that the crystals grown in the sediment after centrifugation consist of a random stacking of close packed layers, whereas the structure produced at 1 g shows indications for fcc stacking.

The sedimentation–diffusion equation presented here does not take into account crystallization. As a rough indication of the effect of crystallization, for $\phi \sim 0.3$ the value of Z calculated with Eq. (16) would be lower by a factor of 2 for the fcc crystal compared to the amorphous structure. The effect of crystallization on the equilibrium volume fraction profile is discussed in Sec. V and a calculated profile is shown in Fig. 9. The degree of ordering is a function of height in the sample as well as of time. Therefore, a more realistic description of the sediment is hard to achieve.

More information about the density profile can be obtained from the present data when an accurate expression for $S(K)$ of a concentrated, disordered suspension of charged particles is available. For a quantitative comparison with calculated density profiles all particle properties, including the double layer parameters, would have to be determined in an independent way. Better techniques exist for the measurement of density profiles, such as x-ray attenuation,[8] but then no information about structure is obtained. Such techniques would allow a quantitative test of the expressions for the osmotic equation of state and the mobility.

In summary, we have presented a light scattering study of the expansion of a compressed sediment of charged spheres. A sedimentation–diffusion equation is used that gives an almost quantitative description of the time evolution of the volume fraction profile. Crystallization occurs only near the top of the sediment due to the strong concentration dependence of this process.

ACKNOWLEDGMENTS

One of the authors (J. vD.) wishes to thank Dr. A. P. Philipse and Dr. Y. D. Yan for several stimulating discussions. We are indebted to G. Harder and M. van Amerongen for skillfully constructing the light scattering setup.

[1] J. Perrin, J. Phys. (Paris) **9**, 5 (1910).
[2] H. Fujita, *Foundations of Ultracentrifugal Analysis* (Wiley, New York, 1977).
[3] P. D. Ross and A. P. Minton, J. Mol. Biol. **112**, 437 (1977).
[4] A. Vrij, J. Chem. Phys. **72**, 3735 (1977).
[5] J. L. Barrat, T. Biben, and J. P. Hansen, J. Phys. Condens. Matt. **4**, L11 (1992).
[6] A. Einstein, Z. Elektrochem. **14**, 235 (1908), reprinted in A. Einstein, *Investigations on the Theory of Brownian Movement,* edited by R. Fürth (Dover, New York, 1956).
[7] K. E. Davis and W. B. Russel, Phys. Fluids A **1**, 82 (1989).
[8] K. E. Davis, W. B. Russel, and W. J. Glantschnig, J. Chem. Soc., Farad. Trans. **87**, 411 (1991).
[9] P. N. Pusey, in *Liquids, Freezing and Glass Transition,* edited by J. P. Hansen, D. Levesque, and J. Zinn-Justin (Elsevier, Amsterdam, 1991), pp. 763–942.
[10] K. E. Davis and W. B. Russel, Adv. Ceram. **21**, 573 (1987).
[11] S. Emmett, S. D. Lubetkin, and B. Vincent, Coll. Surf. **42**, 134 (1989).
[12] K. E. Davis, W. B. Russel, and W. J. Glantschnig, Science **245**, 507 (1989).
[13] S. D. Lubetkin, D. J. Wedlock, and C. F. Edser, Coll. Surf. **44**, 139 (1990).
[14] L. V. Woodcock, Ann. N. Y. Acad. Sci. **371**, 274 (1981).
[15] C. F. Tejero, J. F. Lutsko, J. L. Colot, and M. Baus, Phys. Rev. A **46**, 3373 (1992), and references therein.
[16] M. O. Robbins, K. Kremer, and G. S. Grest, J. Chem. Phys. **88**, 3286 (1988).
[17] E. J. Meijer and D. Frenkel, J. Chem. Phys. **94**, 2269 (1991).
[18] G. J. Hooyman, H. J. Holtan, P. Mazur, and S. R. de Groot, Physica **19**, 1095 (1953).
[19] M. M. Kops-Werkhoven, A. Vrij, and H. N. W. Lekkerkerker, J. Chem. Phys. **78**, 2760 (1983).
[20] W. B. Russel, D. A. Saville, and W. R. Scholwalter, *Colloidal Dispersions* (Cambridge University, Cambridge, 1989).
[21] E. J. W. Verwey and J. T. G. Overbeek, *Theory of the Stability of Lyophobic Colloids* (Elsevier, New York, 1948).
[22] D. Thirumalai, J. Phys. Chem. **93**, 5637 (1989).
[23] H. S. Kang, C. S. Lee, T. Ree, and F. H. Ree, J. Chem. Phys. **82**, 414 (1985).
[24] A. Rahman, M. J. Mandell, and J. P. McTague, J. Chem. Phys. **64**, 1564 (1976).
[25] K. R. Hall, J. Chem. Phys. **57**, 2252 (1972).
[26] A. P. Philipse and C. Pathmamanoharan, J. Coll. Int. Sci. **159**, 96 (1993).
[27] U. Genz and R. Klein, Physica A **171**, 26 (1991).
[28] D. Thies-Weesie and A. P. Philipse (unpublished).
[29] A. P. Philipse and A. Vrij, J. Coll. Int. Sci. **128**, 121 (1989).
[30] A. Vrij *et al.*, Faraday Discuss. Chem. Soc. **90**, 31 (1990).
[31] Y. D. Yan and J. K. G. Dhont, Physica A **198**, 46 (1993).
[32] D. Frenkel and A. J. C. Ladd, J. Chem. Phys.**81**, 3188 (1984).
[33] Y. Monovoukas and A. Gast, J. Colloid Interface Sci. **128**, 533 (1989).
[34] P. N. Pusey *et al.*, Phys. Rev. Lett. **63**, 2753 (1989).
[35] A. J. C. Wilson, *X-ray Optics* (Methuen, London, 1949), Chap. 5.
[36] J. K. G. Dhont, C. Smits, and H. N. W. Lekkerkerker, J. Colloid Int. Sci. **152**, 386 (1991).
[37] A. P. Philipse and A. Vrij, J. Chem. Phys. **88**, 6459 (1988).
[38] P. N. Pusey and W. Van Megen, *Properties of Concentrated Suspensions of Slightly Soft Colloidal Spheres,* in *Physics of Complex and Supramolecular Fluids,* edited by S. A. Safran and N. A. Clark (Wiley, New York, 1987), pp. 673–698.
[39] W. B. Russel, Phase Trans. **21**, 127 (1990).